J. Earth Syst. Sci. (2022)131 60
https://doi.org/10.1007/s12040-022-01816-1

Impacts of sea-surface temperatures on rapid intensification and mature phases of super cyclone Amphan (2020)

Vijay Vishwakarma[1], Sandeep Pattnaik[1,*], Tapajyoti Chakraborty[1], Sudheer Joseph[2] and A K Mitra[3]

[1]*School of Earth Ocean and Climate Sciences, Indian Institute of Technology Bhubaneswar, Argul, Khurda 752 050, Odisha, India.*
[2]*Indian National Centre for Ocean Information Services (INCOIS), Hyderabad, India.*
[3]*National Centre for Medium Range Weather Forecasting (NCMRWF), Noida, India.*
**Corresponding author. e-mail: spt@iitbbs.ac.in*

MS received 2 May 2021; revised 28 October 2021; accepted 1 November 2021

Tropical cyclone rapid intensification (RI) is a major challenge to operational forecasters. Amphan was the most deadly cyclone over the north Indian Ocean basin as it caused 128 deaths in the region. This study aimed to understand the impacts of sea-surface temperatures (SSTs) generated from two leading operational agencies (i.e., Indian National Centre for Ocean Information Services (INCOIS) and National Centre for Medium-Range Weather Forecasting (NCMRWF)) in India on the RI and mature super cyclonic (SuCS) phases of the Amphan (2020) using the weather research and forecasting (WRF4.0) model. Three experiments were carried out using SSTs from INCOIS (INC), NCMRWF (NCM) and control (CNT) with an identical configuration at 3 km resolution with a lead time of up to 96 h. The results suggest that INC offered the best forecast in terms of track, intensity, RI and structure during the three different phases of the SuCS, i.e., RI, mature and weakening stages. The CNT yielded forecasts with the highest errors. The results of the model are validated with *in-situ* buoy and radar observations establishing that INC robustly captured the intensification rate and the structure compared to NCM and CNT. It is also revealed that 30–120 km radii are the key eyewall region contributing to the RI and mature phase of the SuCS Amphan through diabatic heating and convective bursts. The diabatic heating has been placed between 600 and 400 hPa near the eyewall region, and it is well supported by the formation of frozen hydrometeors in the SuCS. INC simulation is able to bring out those features accurately, leading to better intensity prediction, whereas NCM and CNT overestimated those features resulting in unrealistic intensification in the simulations. This study has a direct consequence to the operational forecasting agencies and disaster managers for policy and preparedness.

Keywords. Super cyclone; parameterisation; diabatic heating; WRF.

Supplementary materials pertaining to this article is available on the *Journal of Earth System Science* website (http://www.ias.ac.in/Journals/Journal_of_Earth_System_Science).

Published online: 26 February 2022

1. Introduction

Indian subcontinent frequently suffers from tropical cyclone (TC) landfall. It is one of the most destructive extreme weather events that significantly impact people, economy and environment, particularly in coastal states during the landfall. Over the north Indian Ocean (NIO) basins, TCs develop during the pre-monsoon (March–May) and post-monsoon (October and November) (IMD 2020a, b). Emanuel (2005) noted that there is an increasing trend in the more destructive TCs. Hence, an accurate forecast of TC track, intensity (rate of intensification) and associated rainfall is essential for better disaster preparedness and management. The TC track forecast has improved due to advancement in computing infrastructure, numerical modelling and data assimilation, but the intensity forecast is still a challenging problem (Bender and Ginis 2000; Krishnamurti *et al.* 2005; Rogers *et al.* 2006; Rappaport *et al.* 2009). Inadequate understanding of physical processes during intensity change (Davis and Bosart 2002; Wang and Wu 2004) and improper physical parameterisation in numerical models (Karyampudi *et al.* 1998; Houze *et al.* 2006) make the TC intensity forecast more complex. This complexity further enhances during the rapid intensification (RI) phase of the storm. The air–sea energy exchange in the TC plays a crucial role in its intensity change (Malkus and Riehl 1960; Black and Holland 1995). The change in TC intensity is very much affected by the multi-scale nonlinear interactions of different phenomena and variables, e.g., sea-surface temperature (SST), ocean heat content, vertical wind shear, environmental moisture, inner-core dynamics and thermodynamics, cloud microphysics and air–sea interaction processes (Wang and Wu 2004; Pattnaik and Krishnamurti 2007; Pattnaik *et al.* 2010; Kutty and Gohil 2017; Xu and Wang 2018; Baisya *et al.* 2020; Munsi *et al.* 2021).

The SST of about 26.5°C or above is among the most favourable conditions required for the genesis of a TC (Palmen 1948; Gray 1998). The warm ocean acts as a source of energy, e.g., sensible and latent heat, which are required to maintain the pressure gradient force within the TC core (Malkus and Riehl 1960). Kaplan and DeMaria (2003) showed that ocean inner-core processes and environmental interaction together play an important role in modulating TC intensity. A reasonable prediction of the inner-core structural change and storm radius may improve the forecast of TC intensity, intensity change and RI (Rappaport *et al.* 2009; Chen 2011). It is a well-established fact that a pre-existing high-SST anomaly at the right side of the TC track contributes to RI by inducing latent heat flux (LHF) (Kafatos *et al.* 2006). Using satellite microwave measurements and buoy observations, similar results are also shown by Sun *et al.* (2007). In addition, they have also noted that the absence of a high SST on the right side of the track reduces the intensification process. Crnivec *et al.* (2016) compared the effect of varying SST and the latitude and showed that the intensification rate of TC strongly depends upon the latitude when the SST is about 26°C, and this dependence reduces with an increase in the SST. However, they found that the TC intensification rate is mainly modulated by an increasing SST for a given latitude. In this context, Smith *et al.* (2014) noted that the TC intensification rate is more rapid at low latitudes. In addition to the impact on intensity, the SST also modulates the TC tracks.

Katsube and Inatsu (2016) have shown that over the western pacific, the movements of TCs are faster over warmer SST regions. Several studies over the Atlantic basins have demonstrated that changes in the SST can modulate the TC intensity by modifying the tropospheric temperature profile (Vecchi and Soden 2007; Ramsay and Sobel 2011; Sun *et al.* 2014). They have also found that the changes in TC activities are controlled by the relative value of the SST (i.e., the local SST relative to its spatial mean in the rest of the tropics) rather than the absolute value of the SST. Hegde *et al.* (2016) have concluded that the warm (cool) Indian Ocean (South China Sea) can substantially enhance (reduce) the intensification of TCs due to enhancement (weakening) of moisture supply in the lower troposphere from the vicinity of the TC centre. Therefore, suggesting an important role due to SST variability within the local as well as in the neighbourhood regions. Warm SST, high relative humidity and low vertical wind shear are the most favourable environmental factors for the RI of TCs (Kaplan and DeMaria 2003; Chen 2011). It is also found that the RI of a TC is strongly affected by the wind-induced surface heat exchange (WISHE) (Emanuel 1986; Rotunno and Emanuel 1987). WISHE describes positive feedback between the wind speed of 10 m above the surface (WS10) and the increase in the surface entropy flux (the sum of sensible and LHF). It has long been accepted that SST is a dominant factor that affects the maximum possible intensity attainable by a storm (Palmen

1948; Emanuel 1987, 1988) and strongly influences the development and intensification of a TC (Shapiro and Goldenberg 1998; Cione and Uhlhorn 2003; Trenberth and Shea 2006). In addition, a number of modelling and observational studies have established the relationship between the change in SST and TC intensity (Ooyama 1969; Demaria and Kaplan 1994; Bosart *et al.* 2000; Shay *et al.* 2000; Cione and Uhlhorn 2003).

In this context, such studies are very limited over the NIO basins, particularly with reference to a TC gaining super cyclonic (SuCS) strength. Rai *et al.* (2016) found that the SST variabilities within the radial extent up to 75 km from the TC centre strongly impact its intensification. Furthermore, they have noted a better results in terms of intensity forecast of the TC through incorporation of high-resolution SST and appropriate planetary boundary layer parameterisation in the WRF model (Rai and Pattnaik 2018; Rai *et al.* 2019). An increase in SST contributes greatly to TC intensification by enhancing convection near the eyewall and weakening it in outer spiral rainbands. A study on Odisha SuCS 1999 has shown that the higher resolution SST facilitates TC intensification (Mandal *et al.* 2007). Bongirwar *et al.* (2011) performed sensitivity experiments using different sets of SST (e.g., satellite-observed microwave SST and weekly averaged Reynold's SST) for two intense TCs formed over the Bay of Bengal (BoB). They have concluded that the satellite-derived SST improves the intensity due to an improved prediction of LHF and sensible heat flux (SHF). Other studies have shown that TC intensity has a strong dependence on SST (Ren *et al.* 2014; Merlis *et al.* 2016; Srinivas *et al.* 2017). Srinivas *et al.* (2017) have demonstrated that warmer sea surface conditions lead to northward deviation of the TC tracks over the BoB.

In general, very limited studies are available that focus on severely rapidly intensified TCs over the NIO basins, and there is a scarcity of studies validating the model results with observations, particularly for a SuCS. The SuCS Amphan is responsible for 128 fatalities and caused the highest colossal economic loss (13.7 billion USD) compared to any TC in NIO basins that hit the Indian coast (https://en.wikipedia.org/wiki/Cyclone_Amphan). In addition, following two key questions that have primarily motivated us for carrying out this study, i.e., (i) how different spatial-resolution SSTs from two operational centres (i.e., Indian National Centre for Ocean Information Services (INCOIS) and National Centre for Medium-Range Weather Forecasting (NCMRWF)) impacted the SuCS Amphan characteristics with special emphasis on its intensity, track and structure during RI and mature phase of a SuCS using forecast data as initial and boundary conditions. (ii) How the eyewall convection, dynamics and thermodynamics of the SuCS structures are modulated by these SSTs and ultimately impact its key structures, particularly during the mature phase of its life cycle. The organisation of the rest of the paper is as follows: i.e., overview of SuCS Amphan (section 2), model and experimental design (section 3), results and discussion (section 4), followed by conclusions (section 5).

2. An overview of the SuCS Amphan (2020)

The SuCS Amphan was the most deadly (13.7 billion USD) TC for the NIO basin (State of World Climate 2020), originated from the remnant of a low-pressure area and occurred in the near-equatorial easterly wave over the south Andaman Sea and adjoining southeast BoB on 13 May (IMD 2020a, b). Furthermore, this is only the second SuCS in the BoB basin after Odisha SuCS 1999. Under favourable environmental conditions, it concentrated into a depression over the southeast BoB in the early morning (0000 UTC) of 16th May and further intensified into a deep depression (DD) in the same afternoon (0900 UTC). It moved northwestwards and intensified into cyclonic storm Amphan (pronounced UM-PUN) over the southeast BoB in the evening (1200 UTC) of 16 May 2020. It underwent RI for the next 24 h and accordingly intensified into a very severe cyclonic storm (VSCS) by the afternoon 0900 UTC of 17 May, extremely severe cyclonic storm in the early hours of 18 May (i.e., 2100 UTC of 17 May) and subsequently into a SuCS storm around noon Indian time (i.e., 0600 UTC of 18 May 2020). This is to underline that during the RI process in Amphan quantitatively the intensity has increased by 55 km/h almost 2.3 times in 24 h, i.e., from 1700 UTC of 17 May to 2100 UTC of 18 May 2020, which is one of the rarest records of intensification in this ocean basin. During the DD and cyclonic phase, the propagation of Amphan was very slow (with the translational speed (TS) up to 5 km/h) on 16–18 May. During the intensification of a cyclone into the SuCS category, the TS of the storm reaches up to 30 km/h before landfall. Furthermore, the storm weakened into a VSCS when it

Table 1. *WRF 4.0 model configuration details.*

	Parent domain	Inner domain
Horizontal resolution (km)	9	3
Vertical levels	53	53
Forecast length (h)	96	96
Time step (s)	30	10
Model forecast output time interval (hourly)	6	1
Planetary boundary layer	Bougeault–Lacarrere Scheme (BouLac) (Bougeault and Lacarrere 1989)	
Microphysics	WRF Double Moment 6-class Scheme (Lim and Hong 2010)	
Long-wave radiation	CAM (Collins *et al.* 2004)	
Short-wave radiation		
Surface layer	MM5 similarity scheme (Paulson 1970)	
Land surface	Unified Noah land-surface model (Tewari *et al.* 2004)	
Cumulus	Kain–Fritsch scheme (Kain 2004)	Explicitly resolved
SST (6 hourly): NCMRWF (NCM), INCOIS (INC)		
Initial and boundary conditions (6 hourly): GFS		

hit the coast of West Bengal and Bangladesh on 1200 UTC of 20 May 2020. The SuCS maintained a wind speed of 155–165 km/h after the landfall with a gust up to 185 km/h over land. It lay over West Bengal as a VSCS, gradually moving north-northeastwards during the late evening to night (i.e., 1200–1500 UTC) of 20 May (IMD 2020a, b).

3. Model and experimental design

The weather research and forecasting (WRF)-advanced research WRF (ARW) 4.0 version model (Skamarock *et al.* 2008) is used to conduct experiments with two-way interactive doubly nested domains having horizontal resolutions of 9 and 3 km. The model has 53 vertical levels, with the top level fixed at 50 hPa. The model integration starts at 0000 UTC of 16 May 2020 and ends at 0000 UTC of 20 May 2020 (before the landfall), and this duration has been selected to investigate the impact of SSTs during the RI and mature phase of the SuCS Amphan. The initial and lateral boundary conditions for the simulations were obtained from the National Centers for Environmental Prediction (NCEP) Global Forecast System (GFS) forecast data with a horizontal resolution of 0.25° × 0.25° at 6 h intervals. The model physics options include Kain–Fritsch (Kain 2004) cumulus for the outer domain (9 km), inner domain (3 km) is explicitly resolved. Detailed model configurations are provided in table 1.

To examine the role of SSTs, we have adopted two indigenously generated SSTs from leading operational centres of India, i.e., the INCOIS, Hyderabad and the NCMRWF. INCOIS uses Modular Ocean Model (MOM – v4.0) to generate SSTs (Ravichandran *et al.* 2013) and NCMRWF uses Nucleus for European Modelling of the Ocean (NEMO – v3.2) model to generate SSTs (Mogensen *et al.* 2012). The INCOIS (NCMRWF) SSTs are available at 0.083° × 0.083° (0.25° × 0.25°) spatial resolution and 6-hourly temporal resolution. Three sensitivity experiments are carried out for SuCS Amphan, i.e., one control (CNT), another with INCOIS SSTs (INC) and the other with NCMRWF SSTs (NCM) (table 2). All the numerical simulations are identical in the configuration except for SST forcing and integrated up to 96 h lead time from the initial condition, i.e., 0000 UTC of 16 May 2020. The India Meteorological Department (IMD) best track, TS, radar reflectivity and intensity (i.e., 10-m maximum sustained wind as MSW and minimum central pressure as MCP) and CPC MORPHing technique 8 km resolution precipitation data (CMORPH 2011) are used to validate the model results. All the results discussed are for the innermost domain (3 km).

Table 2. *Experimental design.*

Sl. no.	Experiment name	Details of the experiment
1	CNT	Default SST
2	INC	INCOIS SST (0.083° × 0.083°)
3	NCM	NCMRWF SST (0.25° × 0.25°)

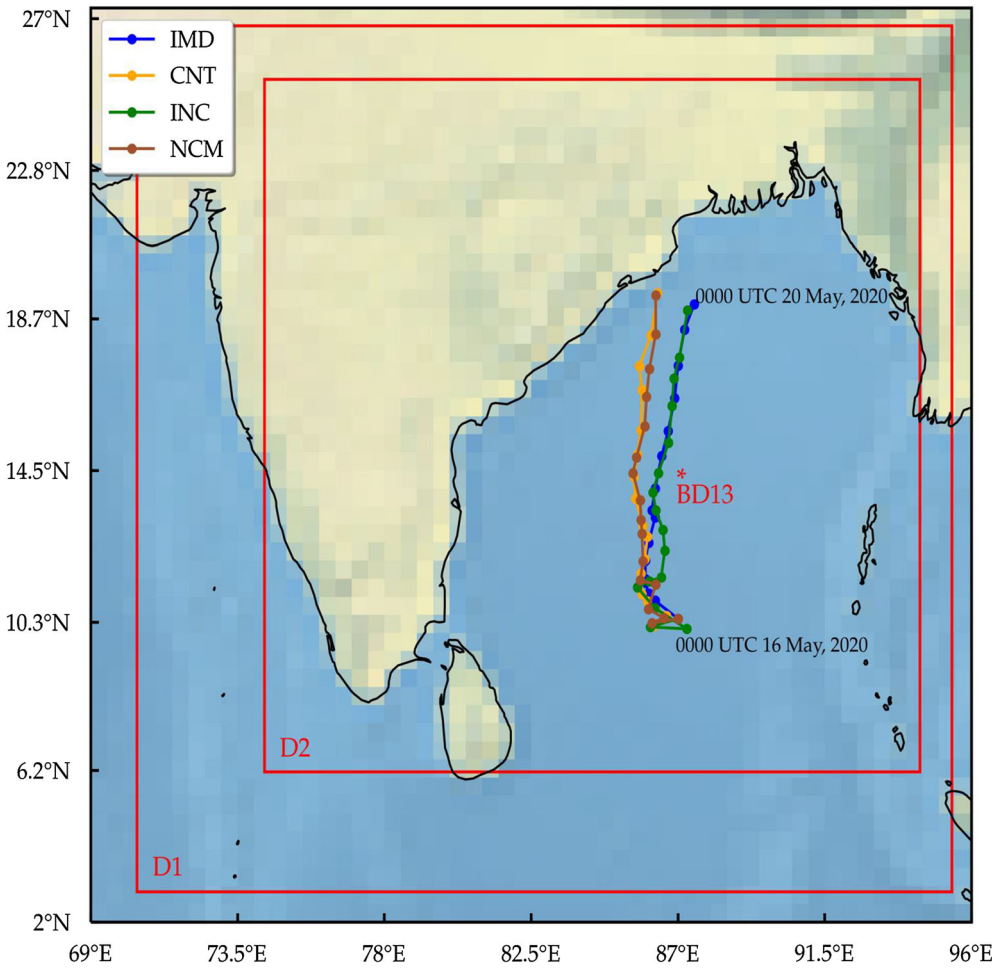

Figure 1. Ninety-six hour forecast tracks (IC: 0000 UTC of 16 May 2020) of SuCS Amphan from simulated experiments, i.e., control (CNT), INCOIS (INC) and NCMRWF (NCM). Observed track from IMD.

4. Results and discussion

In this section, extensive discussions and results are presented concerning the simulated SuCS Amphan's track, intensity, intensity gradient, TS gradient, forecast errors (intensity and absolute track) and vertical–radial cross-section of azimuthally averaged layer anomalous dynamical and thermodynamical parameters, e.g., potential temperature, specific humidity, wind speed, vertical wind speed, radial and tangential wind, diabatic heating, temperature and liquid (e.g., cloud water and rainwater) and frozen (e.g., graupel, snow and ice) hydrometeors. The radial anomalous of parameters are obtained by considering the respective anomalies of the parameters for the SuCS phase (54–75 h) from the mean forecast duration (96 h) at a specific radial distance for each vertical pressure at every forecast hour. This kind of analysis is carried out to provide more insight into key anomalous distribution patterns of parameters to augment our understanding with reference to the fine-scale changes in the eyewall regions impacting characteristics and modulating the intensity of the SuCS. Apart from these parameters, intense convective bursts and diabatic heating processes at different radii are also examined to quantify its contribution towards intensity fluctuations up to 96 h (i.e., 0000 UTC of 16–20 May 2020) for the model inner domain (3 km) covering its RI, mature SuCS and weakening phases.

4.1 *Track and intensity*

The best track (IMD) and simulated track at a 3 h interval of the TC Amphan are presented in figure 1. The best track (IMD) and simulated track are shown at 3 h interval of the TC Amphan in figure 1. In general, the simulations (i.e., CNT, INC and NCM) are able to capture the initial

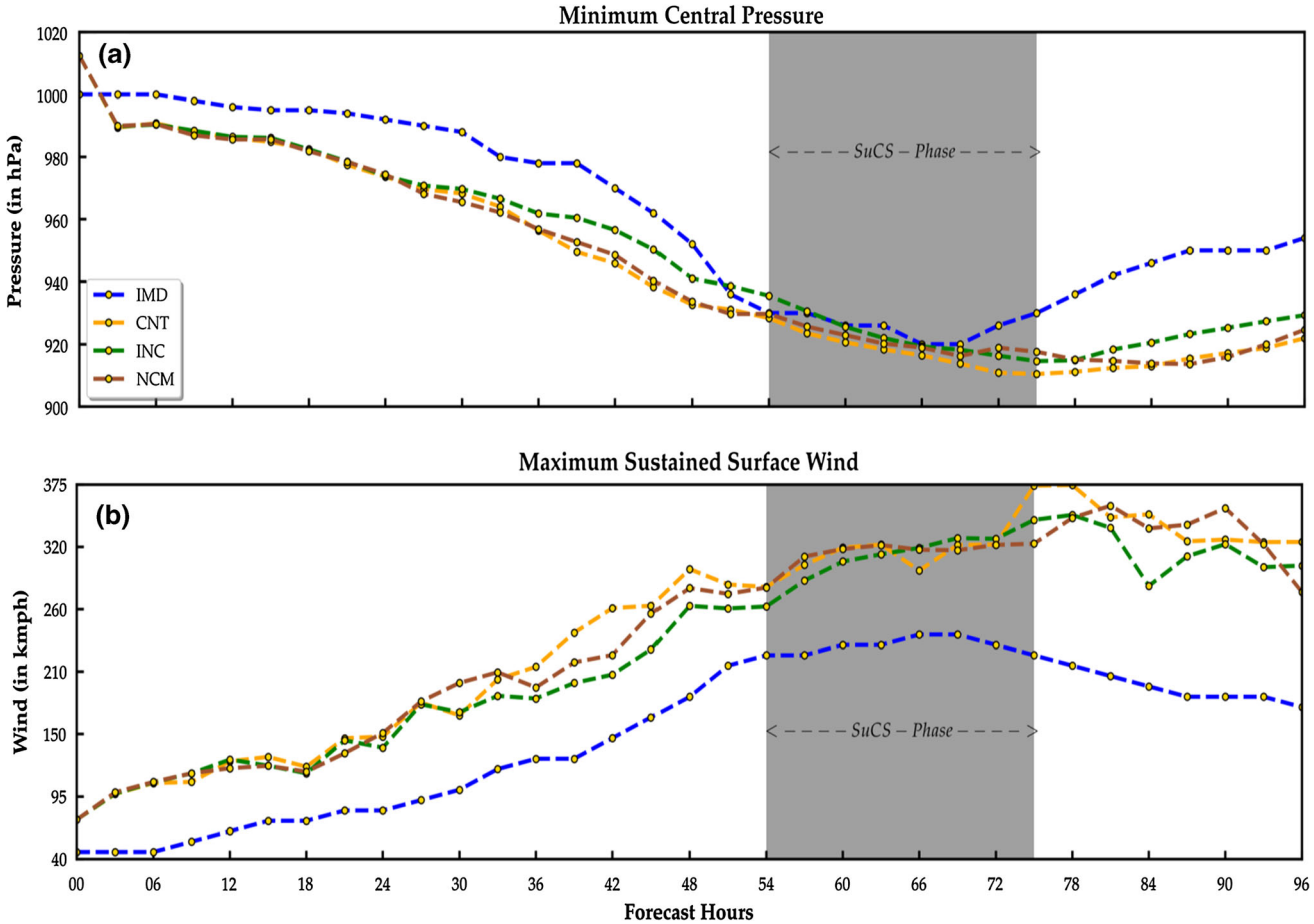

Figure 2. (**a**) MCP (hPa) and (**b**) 10 m maximum wind speed (km/h) of observed (IMD) and simulated (CNT, INC and NCM) experiments.

northwestwards and then eastwards to recurve closer to the IMD. However, NCM and CNT are relatively more westwards of the observed track except INC. In general, the track error increases initially (25–120 km) for the first 12 forecast hours and then starts reducing (120 to 50 km) for all the simulations up to 48 forecast hours (figure 3c). Overall, the variations in track errors for NCM (INC) are between 17.09 and 115.94 km (22.28 and 138.37 km) (figure 1). Furthermore, examining the track forecast errors, it is noted that the NCM track is in closer proximity to the best track compared to INC and CNT. Furthermore, the track error grossly increases after 51 forecast hours in CNT compared to other simulations. In general, among all the three simulations, CNT has the highest track error (90.27 km), followed by INC (68.50 km) and NCM (50.16 km).

The intensity in terms of MSW and MCP is presented in figure 2(a and b) for the 96 h forecast period. The simulated mean intensities of TC wind differ significantly (i.e., 58.58–69.34 km/h) by producing a stronger storm compared to the observation up to 48 h with CNT (INC) having the highest (least) errors and NCM (64.76 km/h) having errors in between these two experiments. However, from 48 to 75 h (RI and SuCS phases), the simulation TC mean intensities converge towards the observations (i.e., 11.56 and 16.57 km/h). Here also, INC (CNT) yielded the best (worst) results with the lowest (highest) errors and NCM (15.48 km/h) being in the middle. Although the large spike in error in the initial hours might be attributed to the model spin-up error, interestingly, INC is able to minimise this error compared to the other two experiments.

Beyond 48 h, the mean error intensity forecast increases rapidly with the maximum magnitudes, i.e., INC (96 km/h), NCM (106 km/h) and CNT (112 km/h) with the highest errors at 87 forecast hours (figure 3b). A similar kind of error pattern is noted for MCP throughout the simulation, with the least errors during the RI phase of the SuCS Amphan for INC (0.98 hPa), NCM (3.98 hPa) and

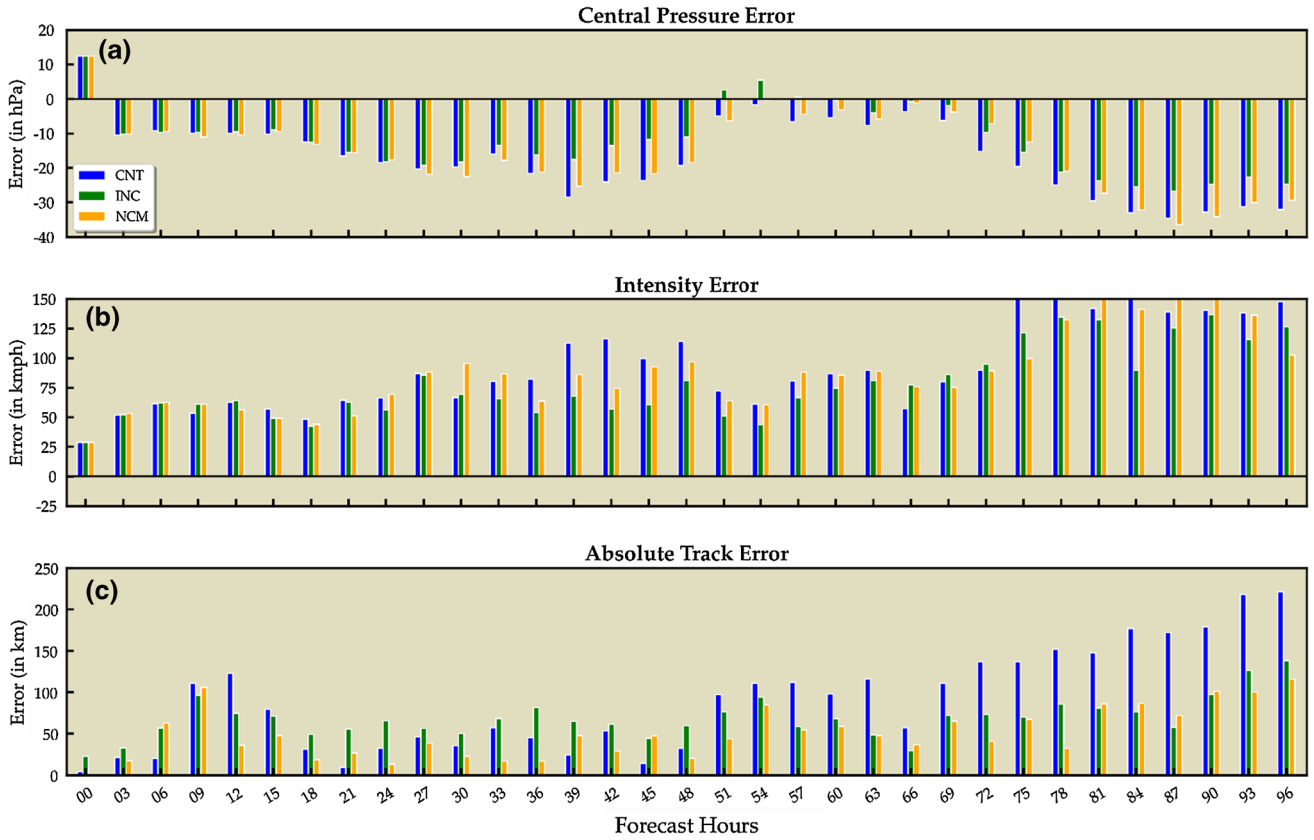

Figure 3. Three hourly forecast errors of simulated experiments (CNT, INC and NCM): (**a**) MCP (hPa), (**b**) 10 m maximum sustained surface wind speed (km/h), and (**c**) absolute track (km).

CNT (6.39 hPa) (figure 3a), and followed by large forecast errors prior and later than this phase. It is evident that among the three simulations, the INC forecast is highly reliable, followed by NCM and CNT (worst). Hence, it clearly suggests the crucial role of including realistic forcing of SSTs to accurately represent the intensification process of the SuCS Amphan over the BoB. Furthermore, this is to highlight that among all the three experiments, INC yielded the least errors compared to NCM and CNT during the RI and SuCS phases. Therefore, a comprehensive analysis is carried out to understand the key processes and mechanisms during this period.

4.2 *Rapid intensification*

The gradients of MCP, MSW and TS at 24 h intervals are presented in figure 4(a–c). As per the IMD criteria, if the TC increases its MSW 30 knots ($\sim$56 km/h) in the last 24 h, then it is considered as the RI phase of the storm (figure 4b). From the results, it is clear that although all the experiments are able to reproduce this significant spike in intensification rate and are within the range of the RI phase (i.e., 30–54 h) with INC (95.59 km/h), NCM (103.55 km/h), CNT (112.07 km/h) and IMD (69.45 km/h). An overestimation in the intensification phase has been observed in all the simulations, with INC (37%) having the least error as compared to NCM (49%) and CNT (61%). Followed by this RI phase, Amphan reached the SuCS stage (i.e., 48–72 h). This is the steady and mature state for the next 24 h. In this duration, NCM (38.72 km/h) again able to yield the best intensity (IMD: 46.3 km/h) while INC (60.11 km/h) and CNT (22.03 km/h) showed underestimation (figure 4b). However, for the overall simulation period INC yielded the best gradient of intensity compared to others. The intensification error magnitudes of RI and mature phases are INC (26.14, 13.81 km/h), NCM (34.1, −7.57 km/h) and CNT (42.62, 24.27 km/h) (figure 4b). As far as MCP gradient is concerned, a similar pattern was also noted in terms of intensity. Here also, the maximum gradients for RI and mature phases for SuCS Amphan are INC (−32.87, −20.77 hPa), NCM (−40.76, −19.23 hPa), CNT (−40.99, −20.61 hPa) and IMD (−40, −11.5 hPa) (figure 4a). This reiterated the fact that INC

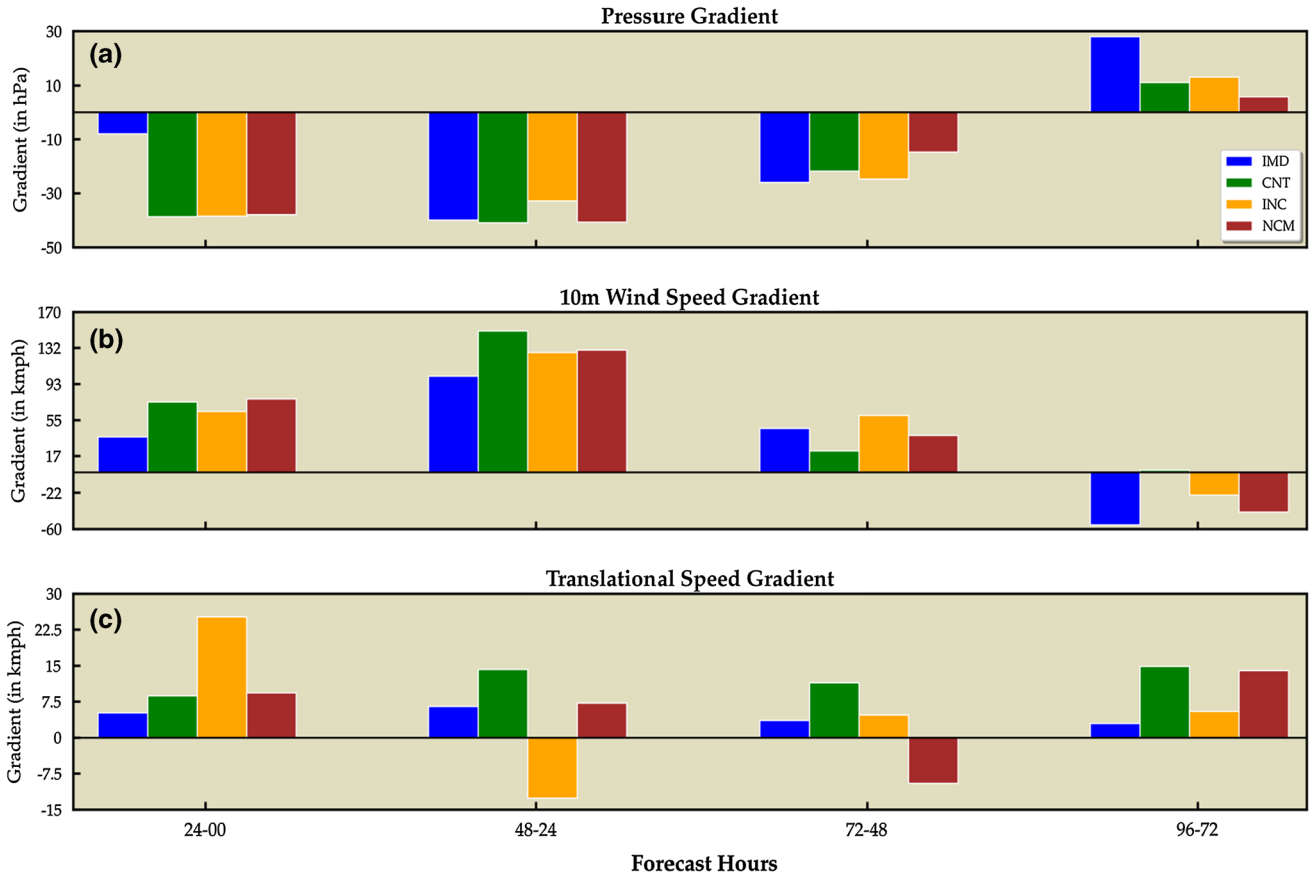

Figure 4. Twenty-four hourly gradients of (**a**) MCP (hPa), (**b**) wind speed gradient (km/h) and (**c**) TS (km/h) from observed (IMD) and simulated experiments (CNT, INC and NCM).

yielded the best simulations followed by NCM. After the 75 h forecast, a sign of the pressure gradient reverses, suggesting that the TC has reduced its intensity. During this phase, the gradients are INC (13.01 hPa), NCM (5.75 hPa), CNT (11.08 hPa) and IMD (28 hPa), suggesting that results from INC are close to the observation in terms of intensity (figure 4a).

The TS gradient of the TC in consecutive 24 h is presented in figure 4(c). In the first 24 h, gradients are overestimated in the simulations compared to observations. The TS gradient for the first two intensification phases are INC (−12.67, 4.72 km/h), NCM (7.2, 9.53 km/h), CNT (14.26, 11.43 km/h) and IMD (5.19, 6.5 km/h). This result suggests that NCM has the least error during 48–72 h; however, overall, INC yielded the least error compared to others. The INC yielded a faster-moving SuCS compared to observations during the initial 24 h. However, in the next 24 h TS gradient suggests, the INC TS gradient becomes negative, suggesting SuCS slows down, whereas the other two simulations CNT and NCM are still showing over-estimated values. It is evident that INC yielded comparatively the best TS during SuCS and beyond (up to 96 h). During the last 48 h of the simulation, INC yielded the least error, i.e., 4.72 and 5.52 km/h, followed by NCM having −9.52 and 13.99 km/h, and CNT 11.43 and 14.87 km/h, and IMD it is 3.56 and 2.93 km/h. Overall, we have noted that mean TS gradients for different experiments are INC (5.68 km/h), NCM (5.26 km/h), CNT (12.23 km/h) and IMD (4.54 km/h). Overall, we have noted that mean TS gradients for different experiments during the SuCS phase are INC (15.46 km/h), NCM (16.46 km/h), CNT (21.77 km/h) and IMD (11.97 km/h). Additionally, we have also found a similar pattern in performance forecast for these three experiments, even at 6 hourly intervals (figure S2).

It is suggested that, in general, INC has performed well compared to NCM. Nevertheless, it is evident from these results that TS being one of the key parameters, is not uniformly evolved in each of these simulations and is highly dependent on multiple factors, including intensification rate. In terms of TS, except for initial hours (i.e., up to 48 h), INC has performed better, whereas NCM has

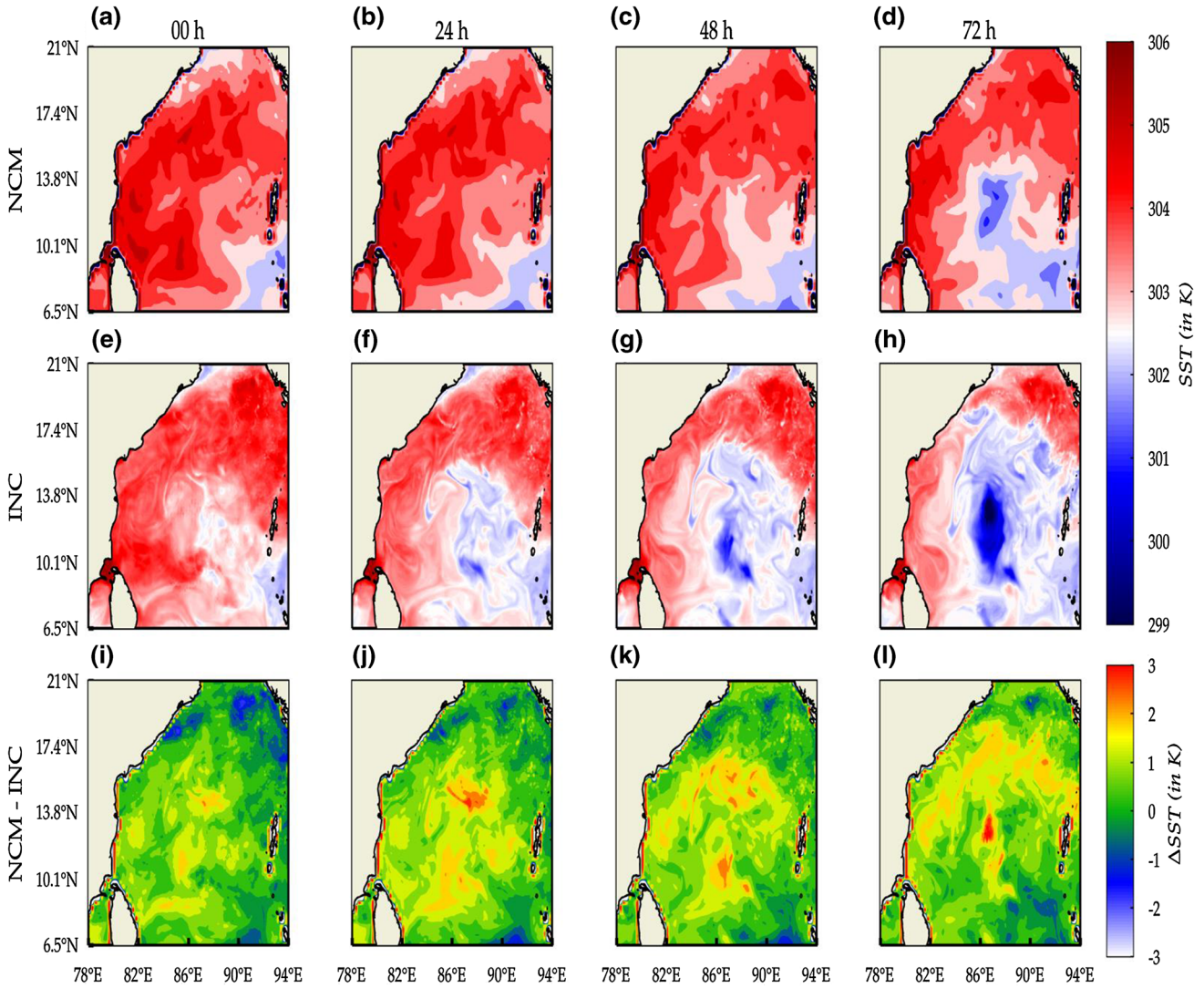

Figure 5. Simulated SST (K) for (**a–d**) NCMRWF (NCM), (**e–h**) INCOIS (INC) and its difference, (**i–l**) NCMRWF (NCM)–INCOIS (INC). First, second, third and fourth columns represent 00, 24, 48 and 72 h.

performed better only during 24–48 h. Overall, CNT has overestimated the TS throughout the simulation hours. NCM shows a closer resemblance to observation only during the RI phase. This clearly demonstrates that INC simulation has led to the best intensity forecast during RI, mature and decay phases of the SuCS Amphan followed by NCM and CNT. This result re-emphasises the fact that accurate and realistic SST is essential to capture not only the RI phase of the SuCS, but also intensity modulation at its different phases during its life cycle.

4.3 *Sea-surface temperature*

SST is one of the potential factors controlling the intensification of the TC. The 24 hourly spatial distribution of the SST for INC and NCM and their differences are shown in figure 5(a–l), respectively. In general, it is noted that NCM has warmer (3 K) SST throughout the simulation on the northern sectors of the TC location compared to INC. The SST cools to about 26°C around the Amphan centre and its neighbourhood regions, which is due to intense churning of water (figure 5d). However, for INC we have noted intense cooling in and around the Amphan from 24 h onwards up to 72 h and over a large area compared to NCM (figure 5e–h). This is to mention that due to the higher resolution of INC SST, we could note finer-scale features of meandering below the SuCS. It is also interesting to note that INC yielded intense cooling up to −2.61°C at the surface, which is realistic compared to the buoy observations. Overall, the difference in the SST results suggests that NCM yielded a warmer ocean condition

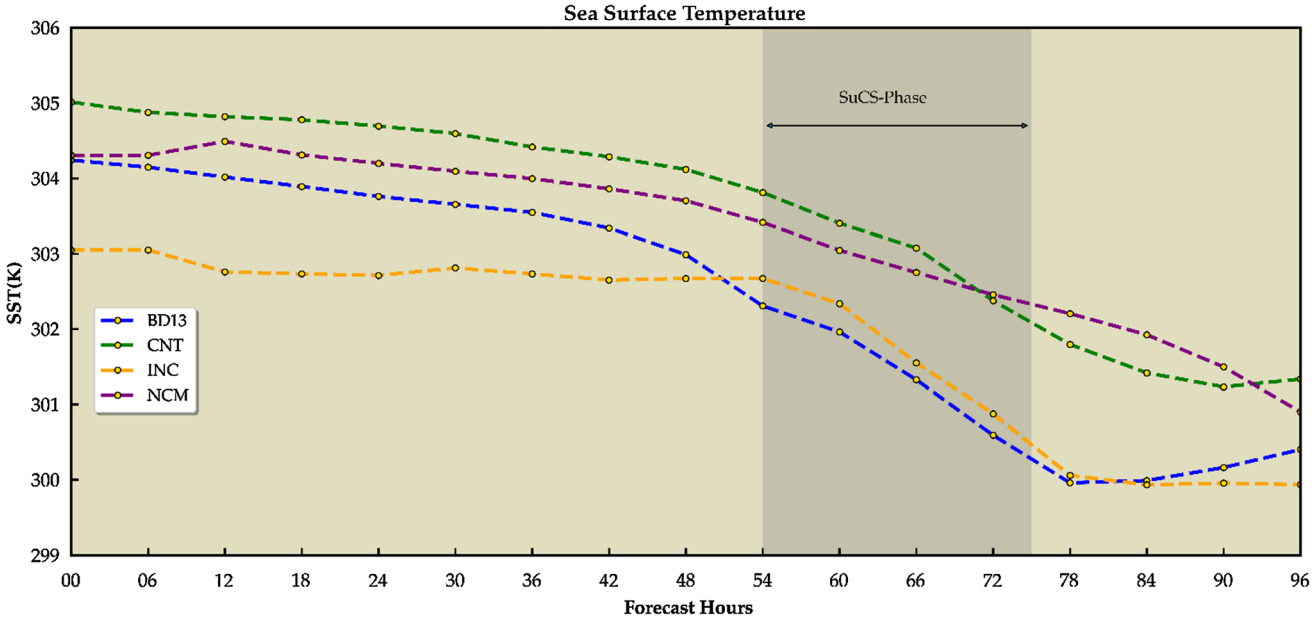

Figure 6. Observed SST (buoy: BD13) along with simulated experiments (i.e., INC and NCM) and CNT.

compared to observation, particularly over the SuCS location, hence suggesting that it might have overestimated the atmosphere–ocean interaction process for the SuCS (figures S4 and S5). It can be observed that during the SuCS phase, the 6 hourly gradients of the SHF and LHF are not well distinct for CNT (figures S4 and S5a–c). However, in the cases of INC (figures S4 and S5d–f) and NCM (figures S4 and S5g–i), it is well spread across the radius up to 300 km in the north and north-eastern quadrants, suggesting that improved air–sea interaction processes being incorporated through SST forcings.

These signatures are clearer when we examined the time-series SST from the buoy (BD13) location (figure S1). The results suggest that throughout the SuCS simulation period, INC yielded more realistic SSTs (closer to BD13 observations) compared to NCM (figure 6). Critically analysing the results, up to 48 h of simulations, we have noted that, on average, NCM has warmer ($\sim$0.5°C) and INC has cooler (~ -0.68°C) SST estimates compared to BD13. Besides, CNT SST is found to be very warm (0.60°C) compared to that of BD13. The pattern of variations up to 48 h in NCM is coherent with the BD13; however, INC has less variability during these hours. The results are distinct after 48 h, i.e., during the SuCS phase, where the gradient of SST is well captured by the INC compared to NCM and CNT. It is to mention that INC elegantly reproduced the realistic SST gradient (-2.61°C) up to 84 h which has almost matched the BD13 (-2.38°C) observations. However, NCM (CNT) simulation has led to less gradient up to -1.21°C (-0.29°C) during that SuCS period. Above all, with reference to BD13, NCM and INC have relatively better signatures of SST compared to CNT. The warmer SST might be one of the major factors of NCM and CNT that has over intensified the Amphan compared to IMD (observation) and INC. Nevertheless, the superior simulation of INC yielded a realistic SST gradient as compared to NCM, particularly during the RI phase, facilitates the intensity fluctuations of the SuCS close to that of observations (IMD) (figure 2a and b).

4.4 *SuCS core structures*

4.4.1 *Dynamical and thermodynamical parameters*

In this section, the mean feature of SuCS Amphan during the 54–75 h forecast is discussed due to its peak intensity. The azimuthally averaged vertical layer anomaly of mean SuCS structures is created up to 300 km from the respective centres of the SuCS at 1 hourly interval (figures 7–9). The purpose of presenting these figures is to capture the distinct signature of core parameters impacting the intensity of the SuCS. The layer anomaly of specific humidity (shading) and wind speed

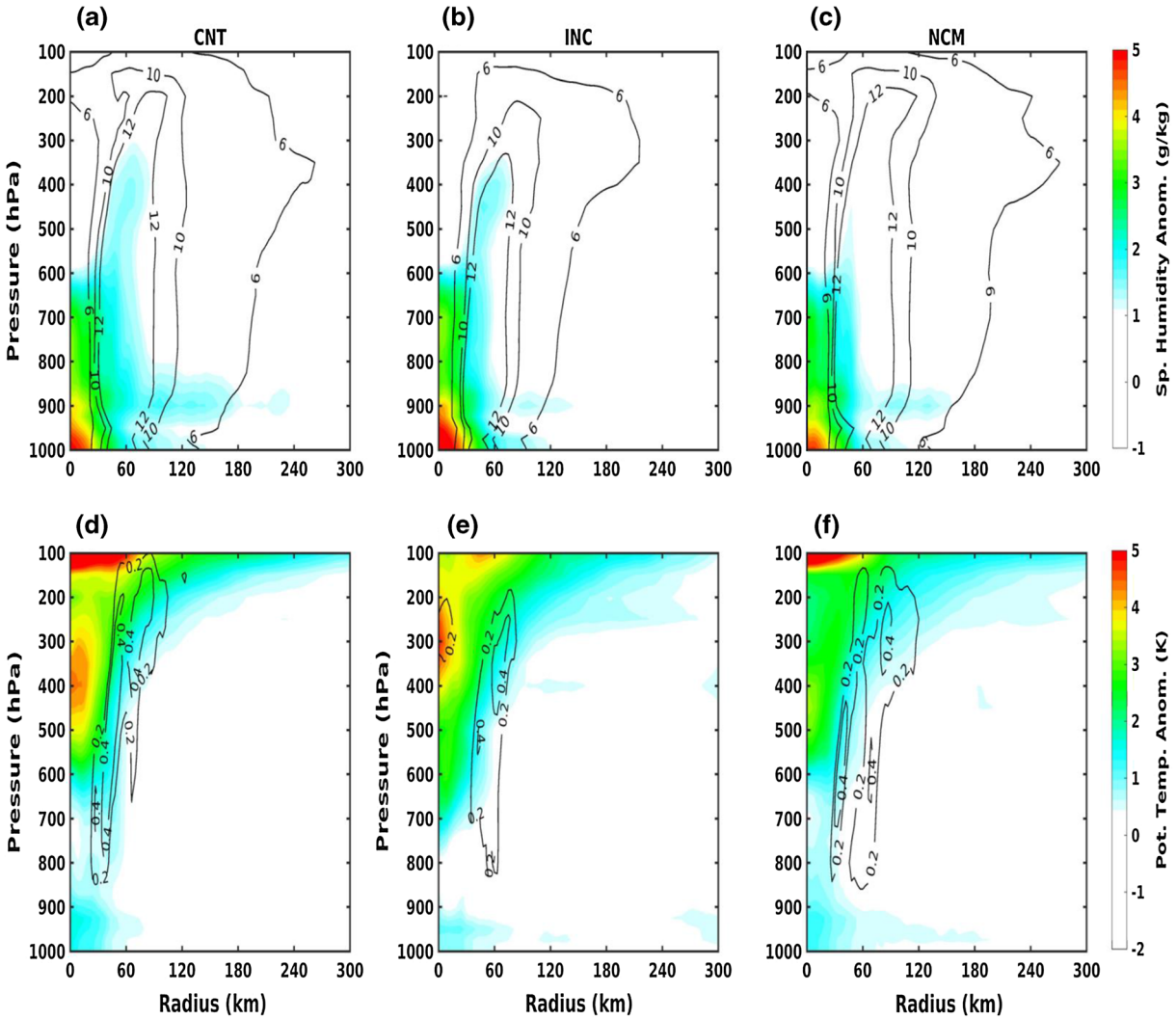

Figure 7. (**a–c**) Layer anomalies of specific humidity (g/kg, shading) and wind speed (m/s, contours), and (**d–f**) potential temperature (K, shading) and vertical wind speed (m/s, contours) during the SuCS phase (54–75 h) of Amphan.

(contour) is shown in figure 7(a–c). In addition, results of potential temperature (shading) and vertical wind speed (contours) are presented in figure 7(d–f).

It is found that maximum anomaly is noted for CNT and NCM has overestimated the wind speed compared to INC. It is also found that the vertical extent of intense wind in CNT and NCM reached higher pressure levels (∼150 hPa) compared to INC, which is restricted up to 400 hPa. Furthermore, the radial extent of wind is found up to 230 and 270 km for CNT and NCM, respectively, compared to 120 km in INC (figure 7a–c). These distinct structures resulted in magnifying the intensity of NCM and CNT compared to INC (figure 2a). Furthermore, it also reiterates that the respective SST forcing plays a key role in determining the intensity of the SuCS. Examining the structure of specific humidity (shadings), it is evident that the radial extent of the specific humidity anomaly is maximum extended up to 120 km for each simulation, but the magnitude of anomalous specific humidity is clearly dominated up to the lowest pressure levels, i.e., 1000–900 hPa (figure 7a–c). It is evident that the vertical extent in terms of the magnitude of anomalous specific humidity is the lowest for NCM compared to INC and CNT. These results suggest that abundant moisture availability is restricted to the eyewall region and at the lower pressure levels closer to the surface, facilitating the intensification of the SuCS.

Examining the anomalous potential temperature (shading) and vertical velocity (contour), it is evident that intense instability has been confined to upper-pressure levels (∼500 hPa and above). However, intense warming (>4 K) has been noted for CNT (figure 7d) around 400 hPa, and for INC about 300 hPa, suggesting that slight upper-level

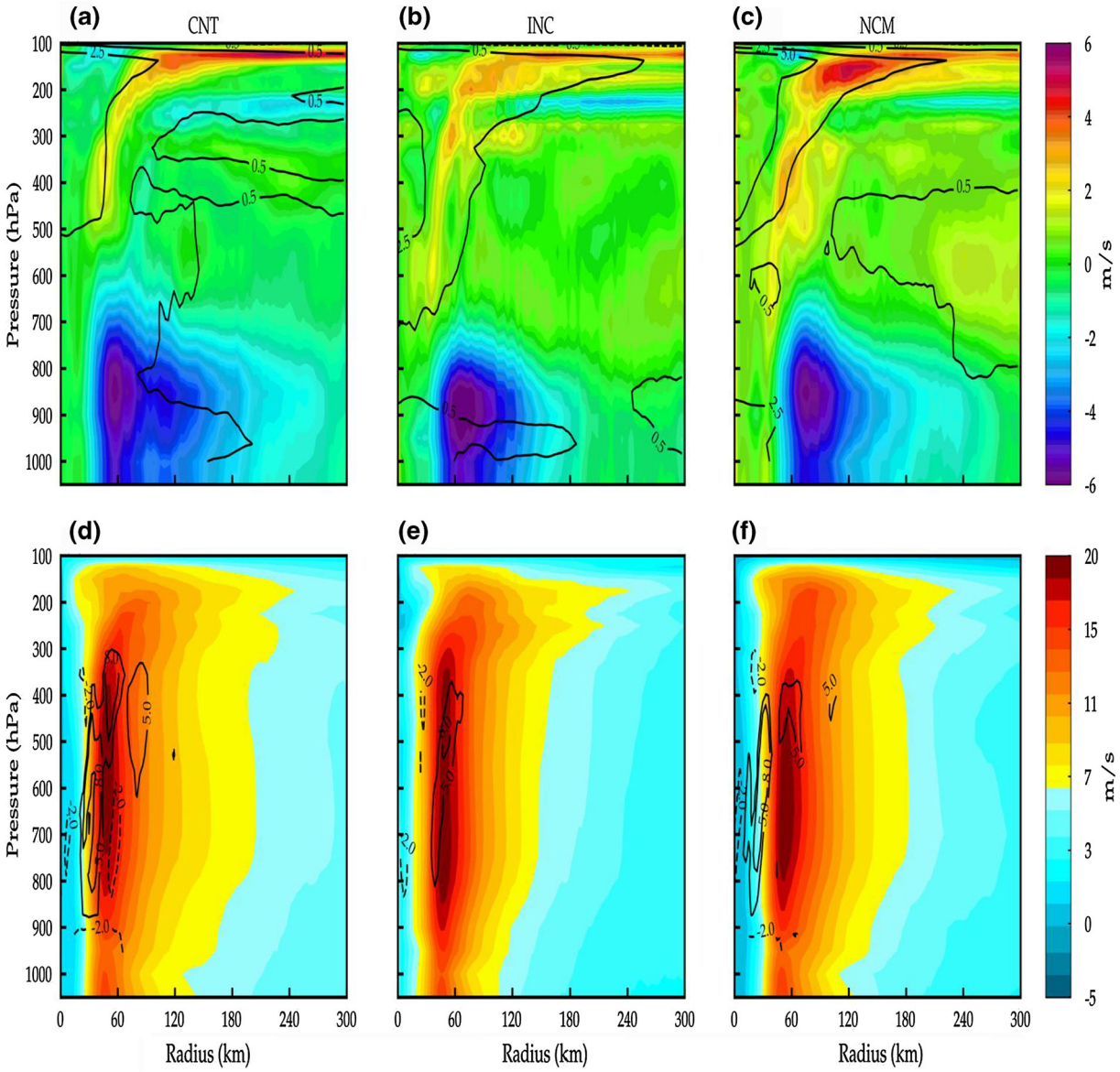

Figure 8. Layer anomalies of: (**a–c**) radial wind (m/s, shading), temperature (K, contours) and (**d–f**) tangential wind (m/s, shading) and diabatic heating (K/h, contours) during the SuCS phase (54–75 h) of Amphan.

warming facilitates the accurate intensification process. Interestingly, NCM simulation is not able to yield middle level (300–500 hPa) heating at the core; rather, an anomalous heating (>4 K) is noted at 100 hPa (figure 7f). A similar pattern of anomalous heating (>4 K) is also noted for CNT at 100 hPa. The vertical velocity anomaly clearly suggests that NCM and CNT have stronger and intense updrafts radially (vertically) extended up to 120 km (100 hPa) compared to INC (radially: 60 km and vertically: 200 hPa) (figure 7d–f). Figure 8(a–c) presents the radial wind (shading) and temperature (contour). The temperature warming up to 0.5 K is largely overestimated in NCM and CNT compared to INC, particularly at the upper-pressure levels (∼500 hPa and above). The overestimation of temperature also radially extended up to 300 km, particularly at the upper-pressure levels. Examining the radial wind, it is evident that an intense inward radial flow (>4–6 m/s) is noted for CNT and NCM, particularly at the lower levels (1000 to 700 hPa) compared to INC. Furthermore, the vertical extent of the radial component of the wind has been observed up to 700 hPa in CNT and NCM compared to INC (800 hPa). The core radial extent of INC is restricted to up to 60 km. At the upper level (500 hPa and above), an enhanced positive anomaly (>4–6 m/s) of radial wind is noted for CNT and NCM compared to INC. The intense outward (inward) anomaly at the

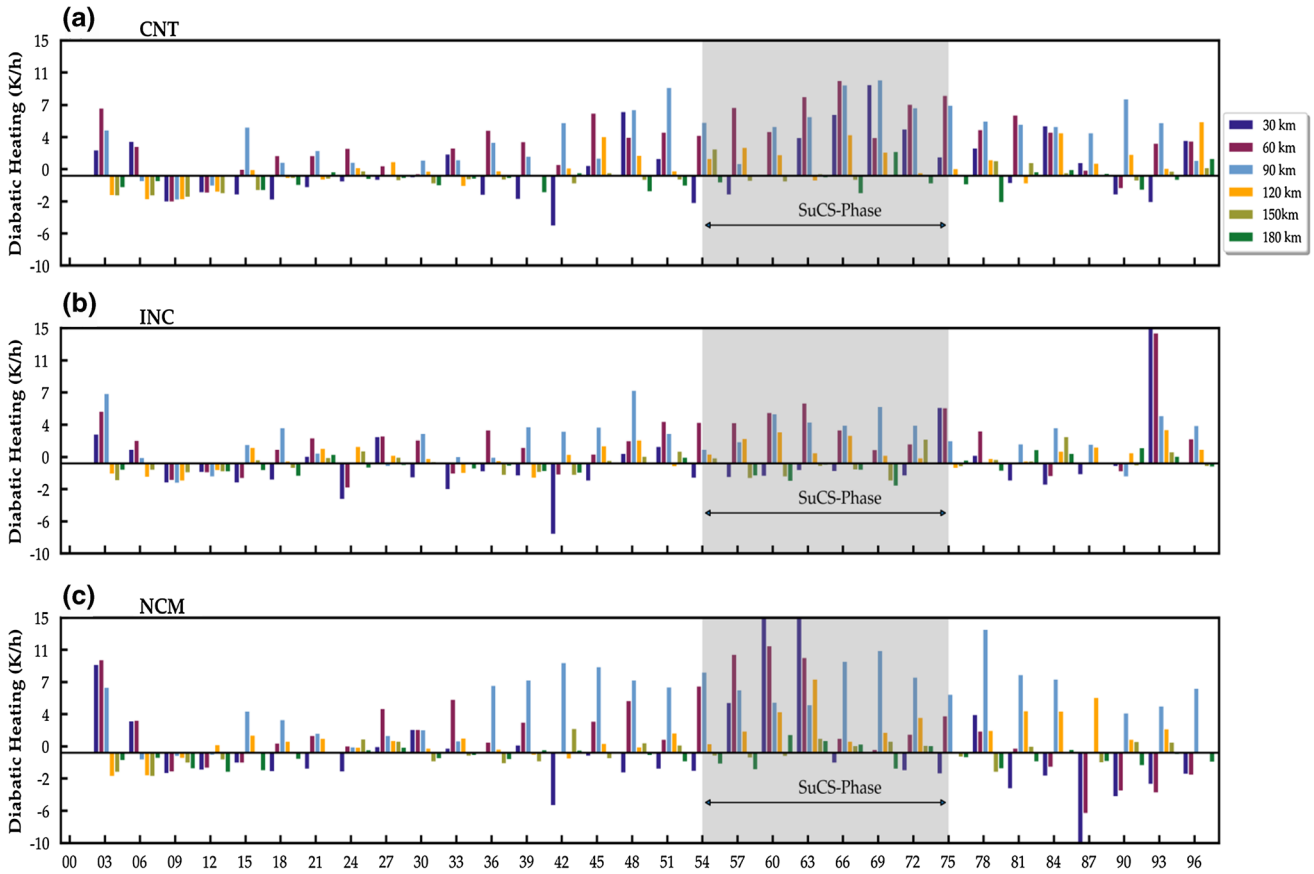

Figure 9. Radial anomalies of diabatic heating (K/h) for (**a**) CNT, (**b**) INC and (**c**) NCM during the 96 h of forecast period for Amphan. Grey-shaded region marked the SuCS phase of the storm.

upper levels (lower levels) of NCM and CNT directly indicates strong upper-level divergence and lower-level convergence in these simulations compared to INC, resulting in more intense SuCS (figure 8a–c).

Furthermore, the anomalies of diabatic heating (contour) and tangential wind (shaded) are shown in figure 8(d–f). The results clearly suggest that an anomalous diabatic heating rate of up to 5 K/h is noted for all three simulations; however, the radial spread of maximum anomalous diabatic heating is noted at 0–75 km for NCM, and at 0–60 km for CNT compared to 30–60 km for INC. This indicates that NCM and CNT have overestimated the diabatic heating resulting in more intensification compared to INC. It also reveals that a narrow and less spread anomalous diabatic heating structure near the eyewall region is key for accurate intensity forecast of the SuCS and well-replicated by INC. For tangential wind (shaded), the maxima have excellent overlapping over the diabatic heating regions. Furthermore, the spread of the anomalous tangential wind (>11 km/h) has been more for CNT (180 km) and NCM (170 km) compared to INC (∼120 km). These results demonstrate that there is a strong coherence of anomalous diabatic heating distribution and the tangential wind efficiently facilitates the warm core structure and RI of the SuCS. Therefore, INC yielded these parameters in a more realistic manner compared to NCM and CNT.

The diabatic heating anomalies at different radial distances (namely at 30, 60, 90, 120, 150 and 180 km) are shown in figure 9(a–c). There is a well-marked increase in the positive anomalies during the SuCS phase at 60, 90 and 120 km radii in the cases of all the simulations. This diabatic heating occurrence closely resembles the convective bursts (discussed in section 4.6). It is evident that the maximum diabatic heating anomaly is intense up to 15 K/h (11 K/h) in NCM (CNT) compared to 7 K/h in INC (figure 9b). This clearly suggests that low-heating tendency in the INC compared to others simulates realistic SuCS Amphan intensity during the RI and mature phases of the TC. Furthermore, similar to convective burst, there is a rapid reduction in diabatic heating of INC, which is still amplified (unrealistic intensification) in the cases of NCM and CNT (figure 9a and c)

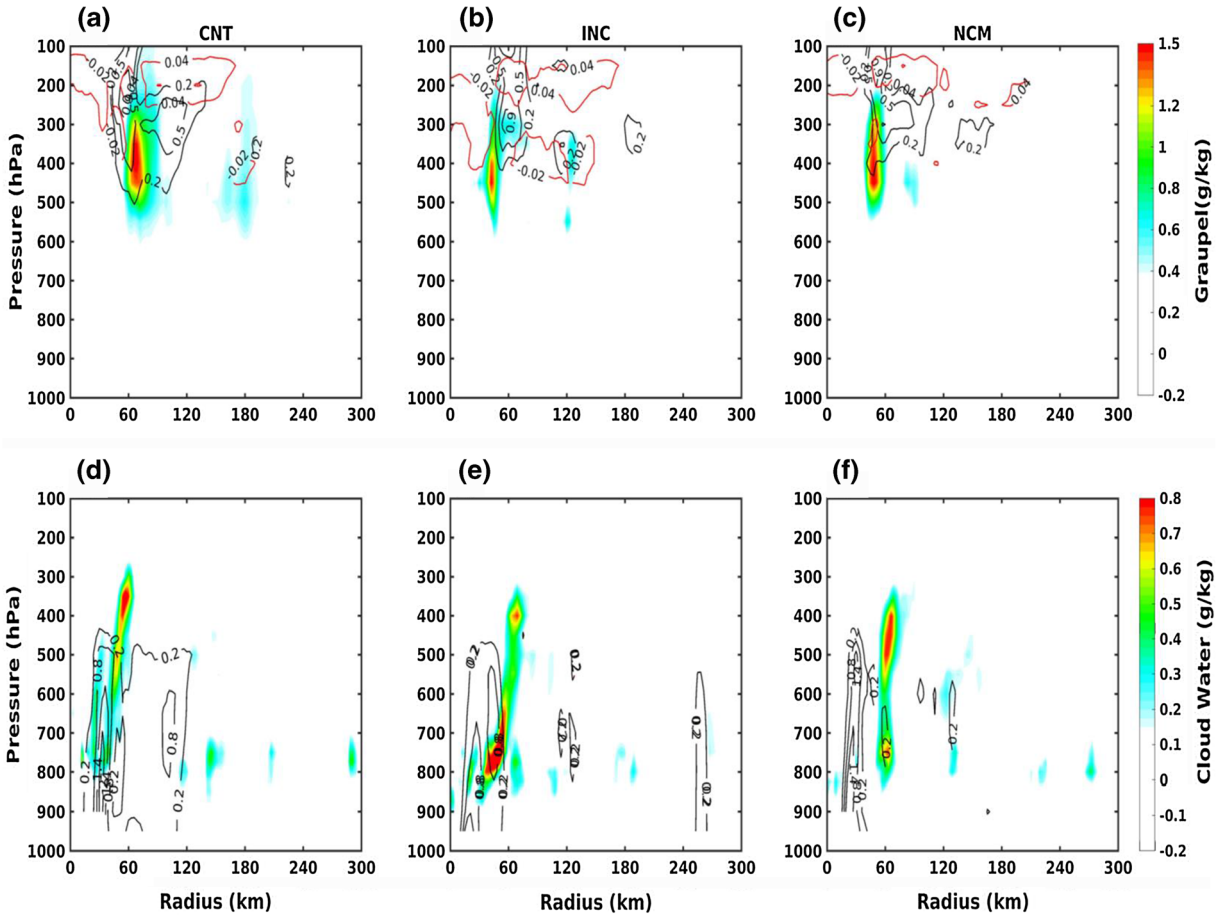

Figure 10. Layer anomalies of (**a–c**) graupel (g/kg, shading), snow (g/kg, black contours) and ice (g/kg, red contours) and (**d–f**) cloud water (g/kg, shading) and rain water (g/kg, contours) during the SuCS phase (54–75 h) of Amphan.

during the weakening phase (beyond 75 h). Overall, there is an excellent coherence between diabatic heating within radii 60–90 km observed to be more efficient in rapidly developing a warm core thermal structure and intense tangential wind shown in figure 8(d–f). In this context, we have examined the height of the cloud bases at different radii and found that during the SuCS phase, the lowest cloud base height is noted for all experiments at 30 km which gradually increases up to 120 km from the centre. After the SuCS phase, the cloud base height at respective radii has shown an increase, indicating the weakening of the TC. These results suggest that the clouds at the nearest radii (30–90 km) with the lowest cloud base heights mainly contribute to diabatic heating and flaring up its intensity (figure S3).

4.4.2 *Hydrometeors*

The vertical–radial structure of anomalous frozen hydrometeors: graupel (shading), snow (black contours) and ice (red contours) during the SuCS phase of the TC for all three simulations are shown in figure 10(a–c). The larger anomaly (>1.5 g/kg) of graupel is evident from CNT and NCM simulations compared to INC. The extent of graupel hydrometeors has a close resemblance with the diabatic heating pattern suggesting its dominant contribution. Ice negative anomaly (>−0.04 g/kg) is present in the case of INC near the centre of the TC between 300 and 400 hPa; however, CNT having a positive anomaly (>0.5 g/kg) suggests that for INC there is a reduction in the ice phase hydrometeors during the SuCS phase. A positive anomaly (>0.02 g/kg) is noted for NCM. Besides, no drastic changes are noted for the snow hydrometeors across the simulations. Hence, the results clearly state that the presence of intense ice and graupel hydrometeors contributes to the storm intensification (figure 10a–c).

Similarly, the vertical–radial structure of anomalous liquid hydrometeors: cloud water (shading) and rainwater (contours) is shown in figure 10(d–f). As compared to INC, CNT and

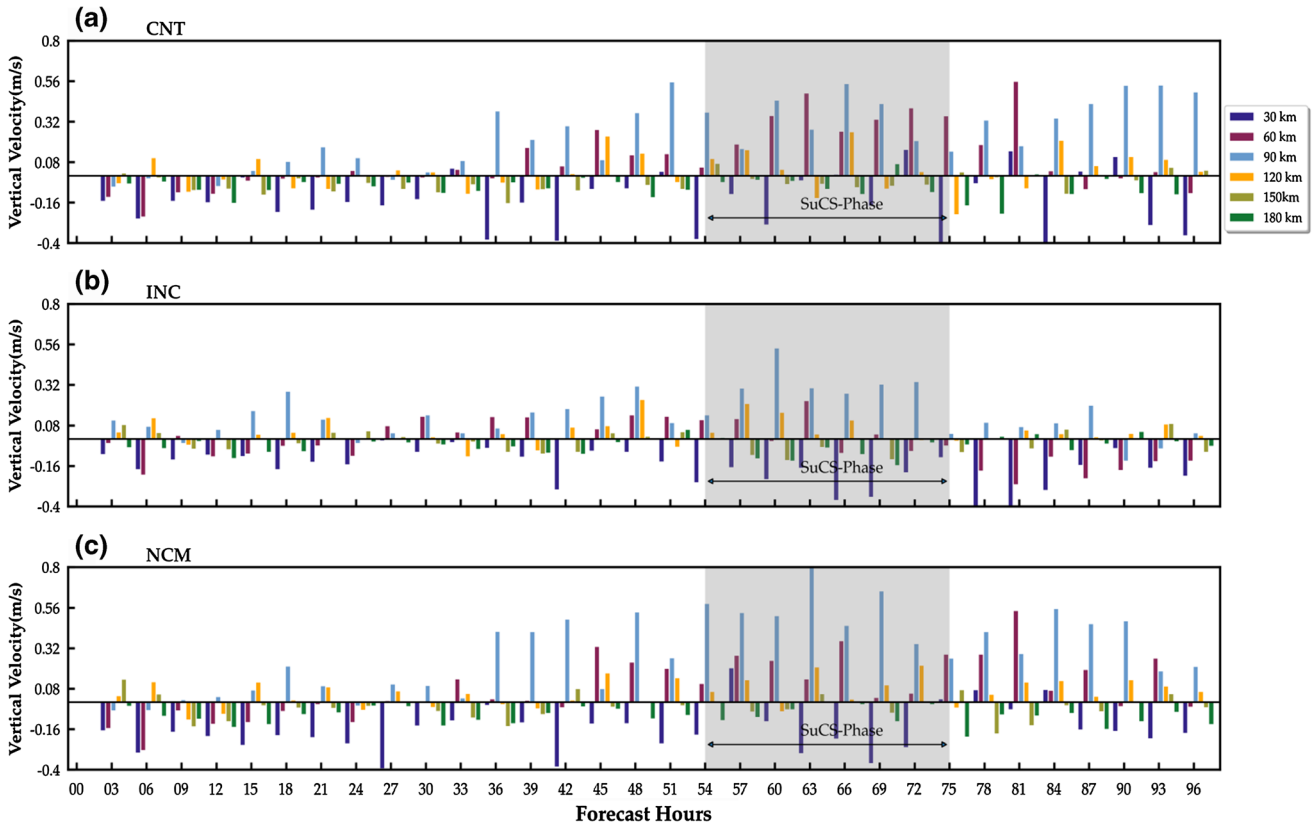

Figure 11. Radial time-series anomalies of vertical wind speed (m/s) (convective bursts) for (**a**) CNT, (**b**) INC and (**c**) NCM during the 96 h of forecast period for Amphan. Grey-shaded region marked the SuCS phase (54–75 h) of the storm.

NCM show a limited radial extent of rainwater with a positive anomaly (>2 g/kg). This suggests that intense rainfall is associated with the narrow core region of the SuCS in CNT and NCM compared to INC. As far as cloud water is concerned, the changes in respective simulations are not that drastic except for INC where the maximum anomaly (>0.8 g/kg) is noted around 800 to 700 hPa suggesting the SuCS holds more precipitable water compared to INC and CNT. To substantiate the hydrometeor distribution, we have examined the cloud base height at different radii (30–180 km) at 30 km intervals for each SuCS simulation (figure S3a–c). In general, it is noted that the cloud base height reduces (50 to ∼1800 km) during the SuCS phase of the storm compared to other phases of the SuCS, and the lowest value is noted for INC simulation (figure S3b). Furthermore, the cloud base height gradually increases with radii, and the maximum height is noted at 180 km. It can be concluded that for INC, higher cloud water content at the lowest level has a close resemblance with the lowest cloud height at small radii (up to 60 km).

4.4.3 *Convective bursts*

The convective bursts within different radii (i.e., 30–180 km at an interval of 30 km) of the SuCS are represented in terms of vertical velocity anomaly (figure 11a–c). The vertical velocity anomaly (convective burst anomaly) has been obtained from the difference between instantaneous and the 96 h mean value (Heng *et al.* 2020; Tang *et al.* 2020). This is to note that only upward velocity (updraft) is considered. The preferential azimuthal location of intense convective burst generally forms over the low shear zone and the structural changes in the vortex due to the vertical stretching are observed (Hazelton *et al.* 2017; Yang *et al.* 2019). It is clearly observed that just before the SuCS phase (36–54 h), the simulations have shown anomalously strong convective bursts (up to 0.6 m/s) over the 60–90 km radii for most of the simulations. The intensity of convective burst is strong for NCM and CNT compared to INC prior to the SuCS phase. This well-marked gradual increase in the convective burst of updrafts until the SuCS phase designates the development of deep convection, vortex strengthening and eyewall development

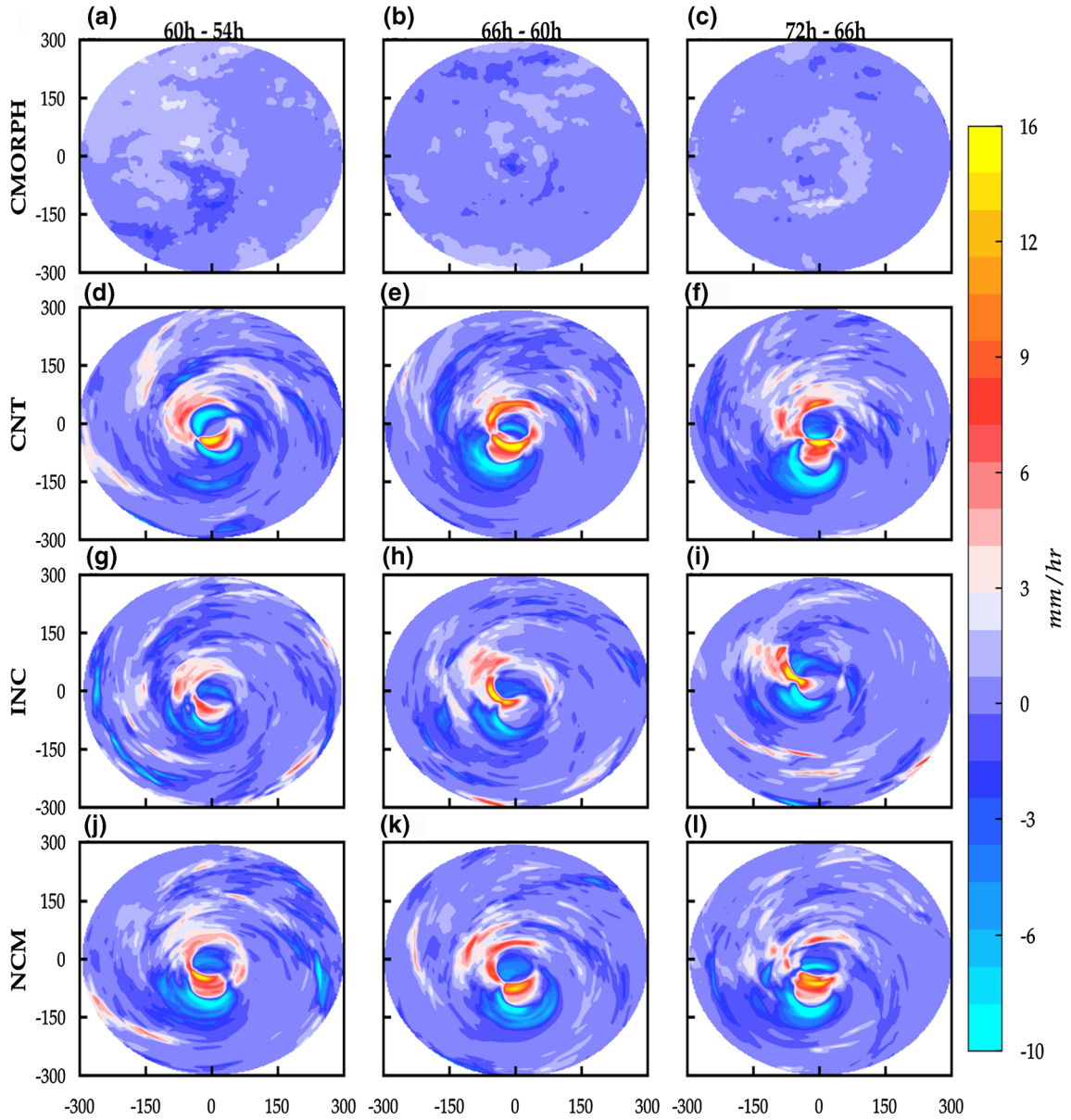

Figure 12. (**a–c**) Observed (CMORPH) and (**d–l**) simulated change 6 hourly rain rate (mm/h) for Amphan.

representing the RI phase. During the SuCS phase, the convective bursts at 60, 90 and 120 km radii are dominated in the cases of CNT and NCM, facilitating the over intensification (figure 2a and b). While in the case of INC, these bursts are limited to 90 km radii, and the burst values at other radii (i.e., 60, 120, 150 and 180 km) are relatively weaker, indicating that INC intensification is less (more realistic) compared to CNT and NCM (figure 2a and b) and this could be one of the factors for the better performance of INC.

In addition, the convective anomaly has been limited to the 0.4 m/s for INC, whereas it has increased up to 0.56 m/s for NCM and CNT, leading to more intensified SuCS in these simulations. We have also noted that 30 km radii have relatively stronger updraft anomalies in the CNT and NCM, suggesting over-intensification. While in the case of INC 30 km radii updrafts, anomalies are either weak or negative (compared to outer radii at 60 and 90 km which correspond to eyewall region of the storm), suggesting a prevalent descending motion associated with the eye of the storm. This again re-establishes the fact that the INC simulated the SuCS phase with higher efficiencies as observed and also suggested that the radius of the eye of the SuCS Amphan is about 25 km (Ahmed *et al.* 2021). In addition to INC, NCM also replicates these

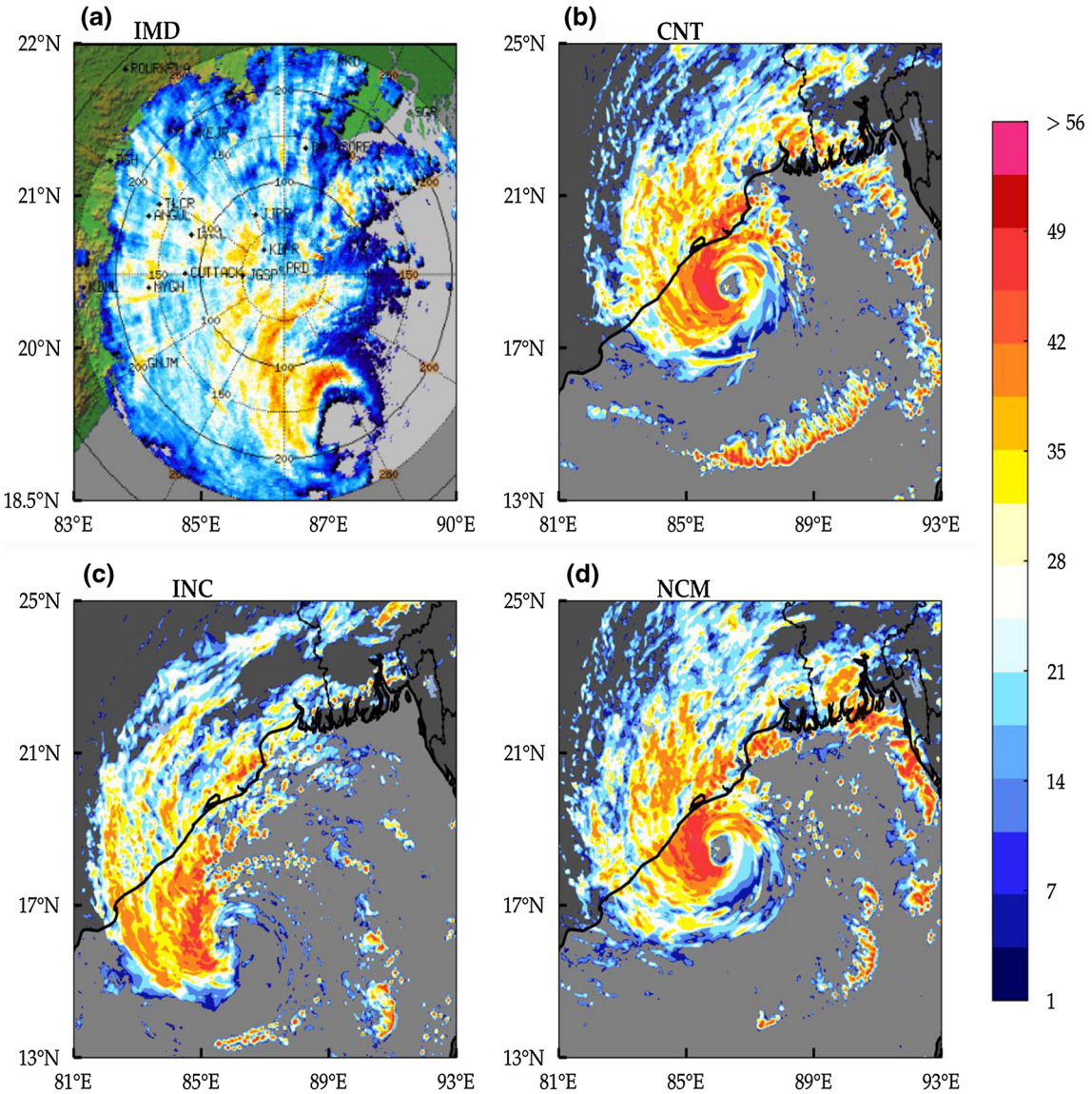

Figure 13. (**a**) Observed and (**b–d**) simulated spatial radar reflectivity (d*bZ*) for Amphan at 2100 UTC of 19 May 2020.

features at 30 km during the SuCS phase; however, for CNT these features are erratic. Just after the SuCS phase (>75 h), there is a rapid fall of convective burst in the INC at different radii with a maximum drop over 30 and 60 km suggesting that the structured eye collapsed in the storm due to weakening (figure 11b). This feature has been completely missed in NCM and CNT, and instead, these two simulations have amplified the convective burst at different radii and thus intensifying the TC, which is unrealistic (figure 11a and c).

4.4.4 *Rainfall and radar reflectivity*

The rates of observed (CMORPH) and simulated rain at 6 hourly intervals during the SuCS phase within a 300 km radius from the centre are presented in figure 12. It is noted that CNT and NCM (figure 12d–f and j–l) yielded intense rainfall (>12 mm/h) with a time up to 150 km radius suggesting stronger TC compared to INC. However, it is also noted that over the southwestern section of the storm, there is a large deficit of up to −10 mm/h as noted for NCM (figure 12j–l) and CNT (figure 12d–f). In the case of INC, we have noted both positive (>6 mm/h) and negative anomalies (3 mm/h) of rainfall moderately and over a limited region (figure 12g–i). These results again suggest that INC has a moderate and realistic structure and intensity of Amphan compared to NCM and CNT. In general, model simulations (CNT, INC and NCM) have overestimated the rainfall and intensity compared to CMORPH during the SuCS phase (figure 12a–c).

Finally, simulated radar reflectivity is validated against IMD Paradip radar at 2100 UTC of 19 May 2020 (figure 13a–d). As anticipated, INC (figure 13c) has nailed the key features of the SuCS core structure compared to NCM (figure 13d) and CNT (figure 13b). INC simulation has realistically reproduced the rugged eyewall region with a reduced intensity as captured by the IMD radar. However, NCM and CNT have shown the well-structured eyewall region with the demarcated eye, suggesting that the TC is still at the intensification stage during that time, and this is contradictory to the observations. As discussed earlier, the TS of INC has been relatively slower compared to that of CNT and NCM. Hence, this result again re-established the fact that the INC yielded the realistic structure, intensity and RI phase of the SuCS storm followed by NCM, whereas CNT has the least efficiency.

5. Conclusions

This study aimed to analyse the impact of SSTs from two leading operational centres (i.e., INCOIS and NCMRWF) on the different phases (RI, mature and weakening) of the SuCS Amphan using the WRF model. In general, the robust impact has been noted on the SuCS structure, intensity and track due to modulation in SST forcing. The model-simulated tracks exhibit early landfall in the cases of CNT and NCM and near-observed landfall timing (minimal errors) in the case of INC. Overall, the track errors are much higher for CNT and marginally higher for INC compared to NCM. In terms of intensity, it is found that, in general, three simulations are able to capture the RI phase (0600 UTC of 17 May to 0600 UTC of 18 May) and mature SuCS phase (0600 UTC of 18 May to 0300 UTC of 19 May 2020); however, INC yielded the best results (least errors) with simulating the intensity accurately even during the weakening phase of the SuCS up to 96 h lead time. By validation with BD13 buoy data, it is also noted that INC yielded the best RI phase of the Amphan with capturing a rapid cooling of SST up to −2.61 K followed by NCM (−1.21 K) compared to observations (−2.38 K). These results clearly demonstrated that the INC integration with higher resolution SST is able to accurately simulate the intensification rate and absolute intensity during RI, mature and weakening phases of the SuCS Amphan, followed by CNT. CNT has failed to simulate the intensification process with the largest errors in its forecast. The gradients of MCP and MSW at 24 h interval matches quite well with those of IMD observations during the RI, SuCS and weakening phases in the case of INC, whereas it has been underestimated for CNT and NCM.

An analysis of the inner-core structure of Amphan during the SuCS phase suggests that the positive radial and tangential wind anomalies superimposed with positive temperature and diabatic heating anomalies extending from the surface to 180 hPa are well simulated by INC, resulting in an accurate intensity forecast compared to NCM and CNT. Both NCM and CNT have overestimated these anomalous structures resulting in an unrealistic higher intensification rate of the TC. Examining the convective burst in the SuCS, it is found that positive anomalies of vertical wind speed and diabatic heating rate for 60 and 90 km radii are dominant during the SuCS phase of the TC in the cases of all the experiments, but INC yielded a moderate vertical convective burst leading to a realistic intensification forecast compared to CNT and NCM. Furthermore, a gradually increasing trend is noted in the case of INC compared to NCM and CNT, where these bursts are highly overestimated, leading to more unrealistic amplification of intensity.

It is found that anomalous liquid and frozen hydrometeors during the SuCS phase suggest that the magnitude of positive graupel anomaly is larger in the cases of CNT and NCM compared to INC. Hence, it is to conclude that this overestimation of frozen hydrometeors might also be responsible for unrealistic intensification in CNT and NCM compared to INC. The results in terms of tangential wind and diabatic heating suggest that 30, 60, 90 and 120 km eyewall radii are the major contributors for the RI and mature phases of the SuCS. This feature is very well simulated by INC compared to NCM and CNT, where these are overestimated by these experiments. Both diabatic heating and convective burst are well poised at the right timings for facilitating the RI and mature SuCS of Amphan. Validation of radar reflectivity with IMD, which is an excellent way to examine the structure of the SuCS from independent observations, also emphasises that INC reproduces the structure compared to NCM and CNT. Although there is a minor mismatch about the location of storm for INC due to slower movement,

the simulated structure is neat and robust. This validation through radar observation is one of the best independent benchmarks to confirm the robustness of the INC forecast.

As far as validation of rain rate is concerned, it is noted that CMORPH observations are not able to bring out the proper structure of a SuCS. Therefore, in intercomparison among the simulations, it is found that NCM and CNT have overestimated the rainfall in the eyewall region compared to INC. Finally, with all the robust supporting evidence, it was demonstrated that INC yielded the best simulation in terms of characteristics of the SuCS Amphan, particularly its RI and mature phases followed by NCM. The CNT forecast has the highest errors. The findings of this study have a direct consequence to the operational forecasting agencies over the Indian region for augmenting its understanding of the key features of the SuCS and its modulations due to the changes in SST forcing. Furthermore, enhanced efficiency of SuCS forecast will facilitate the policymakers, particularly for the coastal states of India, for their better disaster preparedness and minimising the losses in terms of lives and properties.

Acknowledgements

The authors are grateful to the Indian Institute of Technology Bhubaneswar for providing the necessary infrastructure to carry out this research study. We are also grateful to the Council of Scientific and Industrial Research (CSIR) for providing financial support to this study. In addition, we are grateful to the Scientific and Engineering Research Board (SERB) for providing logistics and infrastructure. We extend our sincere gratitude to the Indian National Centre for Ocean Information Services (INCOIS), Hyderabad, the National Centre for Medium-Range Weather Forecasting (NCMRWF), Delhi and India Meteorological Department (IMD) for providing datasets. We are grateful to NCEP-NCAR, CMORPH, for providing the WRF model and data for carrying out this research.

Author statement

VV: Executed the simulation, designing of experiments, carried out the detailed investigation and participated in writing of manuscript. SP: Conceived the research idea, helped in designing the experiments, participated in analysis of results and drafting of the manuscript. TC: Participated in discussion of results. SJ and AKM: Supplied the datasets and participated in discussion.

References

Ahmed R, Mohapatra M, Dwivedi S and Giri R K 2021 Characteristic features of Super Cyclone "AMPHAN"-observed through satellite images; *Trop. Cyclone Res. Rev.* **10(1)** 16–31.

Baisya H, Pattnaik S and Chakraborty T 2020 A coupled modeling approach to understand ocean coupling and energetics of tropical cyclones in the Bay of Bengal basin; *Atmos. Res.* **246** 105092.

Bender M A and Ginis I 2000 Real-case simulations of hurricane-ocean interaction using a high-resolution coupled model: Effects on hurricane intensity; *Mon. Weather Rev.* **128** 917–946.

Black P G and Holland G J 1995 The boundary layer of tropical cyclone Kerry (1979); *Mon. Weather Rev.* **123(7)** 2007–2028.

Bongirwar V, Rakesh V, Kishtawal C M and Joshi P C 2011 Impact of satellite observed microwave SST on the simulation of tropical cyclones; *Nat. Hazards* **58** 929–944.

Bosart L F, Bracken W E, Molinari J, Velden C S and Black P G 2000 Environmental influences on the rapid intensification of Hurricane Opal (1995) over the Gulf of Mexico; *Mon. Weather Rev.* **128(2)** 322–352.

Bougeault P and Lacarrere P 1989 Parameterization of orography–induced turbulence in a Mesobeta-scale model; *Mon. Weather Rev.* **117** 1872–1890.

Chen G 2011 How does shifting Pacific Ocean warming modulate on tropical cyclone frequency over the South China Sea?; *J. Clim.* **24(17)** 4695–4700.

Cione J J and Uhlhorn E W 2003 Sea surface temperature variability in hurricanes: Implications with respect to intensity change; *Mon. Weather Rev.* **131(8)** 1783–1796.

Climate Prediction Center/National Centers for Environmental Prediction/National Weather Service/NOAA/U S Department of Commerce 2011 NOAA CPC Morphing Technique (CMORPH) Global Precipitation Analyses, https://doi.org/10.5065/D6CZ356W, Research Data Archive at the National Center for Atmospheric Research, Computational and Information Systems Laboratory, Boulder, Colorado (Updated daily). Accessed 31 March 2021.

Collins W D, Rash P J, Boville B A, Hack J J, McCaa J R, Williamson D L, Kiehl J T and Briegleb B 2004 Description of the NCAR community atmosphere model (CAM 3.0); NCAR/TN-464?STR, NCAR technical note.

Crnivec N, Smith R K and Kilroy G 2016 Dependence of tropical cyclone intensification rate on sea-surface temperature; *Quart. J. Roy. Meteorol. Soc.* **142** 1618–1627.

Davis C and Bosart L F 2002 Numerical simulations of the genesis of Hurricane Diana (1984). Part II: Sensitivity of track and intensity prediction; *Mon. Weather Rev.* **130(5)** 1100–1124.

DeMaria M and Kaplan J 1994 Sea surface temperature and the maximum intensity of Atlantic tropical cyclones; *J. Clim.* **7(9)** 1324–1334.

Emanuel K A 1986 An air–sea interaction theory for tropical cyclones part I: Steady-state maintenance; *J. Atmos. Sci.* **43(6)** 585–605.

Emanuel K A 1987 The dependence of hurricane intensity on climate; *Nature* **326(6112)** 483–485.

Emanuel K A 1988 The maximum intensity of hurricanes; *J. Atmos. Sci.* **45(7)** 1143–1155.

Emanuel K A 2005 Increasing destructiveness of tropical cyclones over the past 30 years; *Nature* **436(7051)** 686–688.

Gray W M 1998 The formation of tropical cyclones; *Meteorol. Atmos. Phys.* **67** 37–69.

Hazelton A, Rogers R and Hart R 2017 Analyzing simulated convective bursts in two Atlantic hurricanes. Part I: Burst formation and development; *Mon. Weather Rev.* **145** 3073–3094, https://doi.org/10.1175/MWR-D-16-0267.1.

Hegde A K, Kawamura R and Kawano T 2016 Evidence for the significant role of sea surface temperature distributions over remote tropical oceans in tropical cyclone intensity; *Clim. Dyn.* **47** 623–635.

Heng J, Yang S, Gong Y, Gu J and Liu H 2020 Characteristics of the convective bursts and their relationship with the rapid intensification of Super Typhoon Maria (2018); *Atmos. Oceanic Sci. Lett.* **13(2)** 146–154.

Hong S Y, Park H, Cheong H B, Kim J E E, Koo M S, Jang J, Ham S, Hwang S O, Park B K, Chang E C and Li H 2013 The global/regional integrated model system (GRIMS); *Asia-Pac. J. Atmos. Sci.* **49** 219–243.

Houze Jr R A, Chen S S, Lee W C, Rogers R F, Moore J A, Stossmeister G J and Brodzik S R 2006 The hurricane rainband and intensity change experiment: Observations and modelling of Hurricanes Katrina, Ophelia, and Rita; *Bull. Am. Meteorol. Soc.* **87(11)** 1503–1522.

IMD 2020a Super Cyclonic Storm 'AMPHAN' over Southeast Bay of Bengal: A Report. Retrieved from http://www.rsmcnewdelhi.imd.gov.in.

IMD 2020b Cyclone eAtlas; http://www.rsmcnewdelhi.imd.gov.in.

Jimenez P A, Dudhia J, Gonzalez-Rouco J F, Navarro J, Montavez J P and Garcia-Bustamante E 2012 A revised scheme for the WRF surface layer formulation; *Mon. Weather Rev.* **140** 898–918.

Kafatos M, Sun D, Gautam R, Boybeyi Z, Yang R and Cervone G 2006 Role of anomalous warm Gulf waters in the intensification of Hurricane Katrina; *Geophys. Res. Lett.* **33** L17802.

Kain J S 2004 The Kain-Fritsch convective parameterization: An update; *J. Appl. Meteorol.* **43** 170–181.

Kaplan J and DeMaria M 2003 Large-scale characteristics of rapidly intensifying tropical cyclones in the North Atlantic basin; *Wea. Forecasting* **18(6)** 1093–1108.

Karyampudi V M, Lai G S and Manobianco J 1998 Impact of initial conditions, rainfall assimilation, and cumulus parameterization on simulations of Hurricane Florence (1988); *Mon. Weather Rev.* **126(12)** 3077–3101.

Katsube K and Inatsu M 2016 Response of tropical cyclone tracks to sea surface temperature in the western North Pacific; *J. Clim.* **29** 1955–1975.

Krishnamurti T N, Pattnaik S, Biswas M K, Bensman E, Kramer M, Surgi N and Kumar T V 2010 Hurricane forecasts with a mesoscale suite of models; *Tellus A: Dyn. Meteorol. Oceanogr.* **62(5)** 633–646.

Krishnamurti T N, Pattnaik S, Stefanova L, Kumar T S V V, Mackey B P, O'Shay A J and Pasch R J 2005 The hurricane intensity issue; *Mon. Weather Rev.* **133** 1886–1912.

Kutty G and Gohil K 2017 The role of mid-level vortex in the intensification and weakening of tropical cyclones; *J. Earth Syst. Sci.* **126(7)** 1–12.

Lim K S S and Hong S Y 2010 Development of an effective double-moment cloud microphysics scheme with prognostic cloud condensation nuclei (CCN) for weather and climate models; *Mon. Weather Rev.* **138** 1587–1612.

Malkus J S and Riehl H 1960 On the dynamics and energy transformations in steady-state hurricanes; *Tellus A* **12** 1–20.

Mandal M, Mohanty U C, Sinha P and Ali M M 2007 Impact of sea surface temperature in modulating movement and intensity of tropical cyclones; *Nat. Hazards* **41** 413–427.

Merlis T M, Zhou W, Held I M and Zhao M 2016 Surface temperature dependence of tropical cyclone-permitting simulations in a spherical model with uniform thermal forcing; *Geophys. Res. Lett.* **43** 2859–2865.

Mogensen K S, Balmaseda M A and Weaver A 2012 The NEMOVAR ocean data assimilation system as implemented in the ECMWF ocean analysis for system 4; *ECMWF Tech. Memo.* **668**.

Munsi A, Kesarkar A, Bhate J, Panchal A, Singh K, Kutty G and Giri R 2021 Rapidly intensified, long duration North Indian Ocean tropical cyclones: Mesoscale downscaling and validation; *Atmos. Res.* **259** 105678.

Ooyama K 1969 Numerical simulation of the life cycle of tropical cyclones; *J. Atmos. Sci.* **26(1)** 3–40.

Palmen E 1948 On the formation and structure of tropical hurricanes; *Geophysica* **3** 26–38.

Pattnaik S and Krishnamurti T 2007 Impact of cloud microphysical processes on hurricane intensity, part 1: Control run; *Meteorol. Atmos. Phys.* **97** 117–126.

Pattnaik S, Inglish C and Krishnamurti T N 2010 Influence of rain rate initialization, cloud microphysics and cloud torques on hurricane intensity; *Mon. Weather Rev.* **139** 627–649.

Paulson C A 1970 The mathematical representation of wind speed and temperature profiles in the unstable atmospheric surface layer; *J. Appl. Meteorol.* **9** 857–861.

Rai D and Pattnaik S 2018 Sensitivity of tropical cyclone intensity and structure to planetary boundary layer parameterization; *Asia-Pac. J. Atmos. Sci.* **54(3)** 473–488.

Rai D, Pattnaik S and Rajesh P V 2016 Sensitivity of tropical cyclone characteristics to the radial distribution of sea surface temperature; *J. Earth Syst. Sci.* **125** 691–708.

Rai D, Pattnaik S, Rajesh P V and Hazra V 2019 Impact of high-resolution sea surface temperature on tropical cyclone characteristics over the Bay of Bengal using model simulations; *Meteorol. Appl.* **26(1)** 130–139.

Ramsay H A and Sobel A H 2011 Effects of relative and absolute sea surface temperature on tropical cyclone potential intensity using a single-column model; *J. Clim.* **24** 183–193.

Rappaport E N, Franklin J L, Avila L A, Baig S R, Beven J L, Blake E S, Burr C A, Jiing J G, Juckins C A, Knabb R D, Landsea C W, Mainelli M, Mayfield M, McAdie C J, Pasch R J, Sisko C, Stewart S R and Tribble A N 2009 Advances and challenges at the National Hurricane Center; *Wea. Forecasting* **24(2)** 395–419.

Ravichandran M, Behringer D, Sivareddy S, Girishkumar M, Chacko N and Harikumar R 2013 Evaluation of the global ocean data assimilation system at INCOIS: The tropical Indian Ocean; *Ocean Modell.* **69** 123–135.

Ren D, Lynch M, Leslie L M and Lemaeshall J 2014 Sensitivity of tropical cyclone tracks and intensity to ocean surface temperature: Four cases in four different basins; *Tellus A* **66** 24212.

Rogers R, Aberson S, Black M, Black P, Cione J, Dodge P, Gamache J, Kaplan J, Powell M, Dunion J, Uhlhorn E, Shay N and Surgi N 2006 The intensity forecasting experiment: A NOAA multi-year field program for improving tropical cyclone intensity forecasts; *Bull. Am. Meteorol. Soc.* **87(11)** 1523–1537.

Rotunno R and Emanuel K A 1987 An air–sea interaction theory for tropical cyclones. Part II: Evolutionary study using a non-hydrostatic axisymmetric numerical model; *J. Atmos. Sci.* **44(3)** 542–561.

Shapiro L J and Goldenberg S B 1998 Atlantic sea surface temperatures and tropical cyclone formation; *J. Clim.* **11(4)** 578–590.

Shay L K, Goni G J and Black P G 2000 Effects of a warm oceanic feature on Hurricane Opal; *Mon. Weather Rev.* **128(5)** 1366–1383.

Skamarock W C, Klemp J B, Dudhia J, Gill D O, Barker D M, Duda M G, Huang X Y, Wang W and Powers J G 2008 A description of the advanced research WRF Version 3; Technical Report NCAR/TN-475+STR, National Centre for Atmospheric Research, Boulder, CO.

Smith R K, Kilroy G and Montgomery M T 2014 Why do model tropical cyclones intensify more rapidly at low latitudes?; *J. Atmos. Sci.* **72(5)** 1783–1804.

Srinivas C V, Mohan G M, Rao B D V, Baskaran R and Venkatraman B 2017 Numerical simulations with WRF to study the impact of sea surface temperature on the evolution of tropical cyclones over the Bay of Bengal; In: *Tropical cyclone activity over the north Indian Ocean* (eds) Mohapatra M, Bandyopadhyay B K and Rathore L S, Springer, Cham, pp. 259–271.

State of World Climate 2020 WMO Report No. 1264, ISBN: 978-92-63-11264-4.

Sun D, Kafatos M, Cervone G, Boybeyi Z and Yang R 2007 Satellite microwave detected SST anomalies and hurricane intensification; *Nat. Hazards* **43** 273–284.

Sun Y, Zhong Z, Yi L, Ha Y and Sun Y 2014 The opposite effects of inner and outer sea surface temperature on tropical cyclone intensity; *J. Geophys. Res. Atmos.* **119** 2193–2208.

Tang B, Fang J, Bentley A, Kilroy G, Nakano M and Park M 2020 Recent advances in research on tropical cyclogenesis; *Trop. Cyclone Res. Rev.* **9(2)** 87–105.

Tewari M, Chen F, Wang W, Dudhia J, LeMone M and Cuenca R H 2004 Implementation and verification of the unified NOAH land surface model in the WRF model; In: *20th conference on weather analysis and forecasting/16th conference on numerical weather prediction*, pp. 11–15.

Trenberth K E and Shea D J 2006 Atlantic hurricanes and natural variability in 2005; *Geophys. Res. Lett.* **33(12)** L12704.

Vecchi G A and Soden B J 2007 Effect of remote sea surface temperature change on tropical cyclone potential intensity; *Nature* **450** 1066–1070.

Wang Y Q and Wu C C 2004 Current understanding of tropical cyclone structure and intensity changes – A review; *Meteorol. Atmos. Phys.* **87(4)** 257–278.

Xu J and Wang Y 2018 Dependence of tropical cyclone intensification rate on sea surface temperature, storm intensity, and size in the western north pacific; *Wea. Forecasting* **33(2)** 523–537.

Yang S, Tang X, Zhong S, Chen B, Zhou Y, Gao S and Wang C 2019 Convective bursts episode of the rapidly intensified typhoon Mujigae (2015); *Adv. Atmos. Sci.* **36(5)** 541–556.

Corresponding editor: Kavirajan Rajendran